Ecology, 97(7), 2016, pp. 1735–1745

Integrating population dynamics models and distance sampling data: a spatial hierarchical state-space approach

Khurram Nadeem,[1,3] Jeffrey E. Moore,[2] Ying Zhang,[1] and Hugh Chipman[1]

[1]*Department of Mathematics & Statistics, Acadia University, Wolfville, Nova Scotia B4P 2R6 Canada*
[2]*Marine Mammal and Turtle Division, Southwest Fisheries Science Center, NOAA, 8901 La Jolla Shores Drive, La Jolla, California 92037 USA*

Abstract. Stochastic versions of Gompertz, Ricker, and various other dynamics models play a fundamental role in quantifying strength of density dependence and studying long-term dynamics of wildlife populations. These models are frequently estimated using time series of abundance estimates that are inevitably subject to observation error and missing data. This issue can be addressed with a state-space modeling framework that jointly estimates the observed data model and the underlying stochastic population dynamics (SPD) model. In cases where abundance data are from multiple locations with a smaller spatial resolution (e.g., from mark–recapture and distance sampling studies), models are conventionally fitted to spatially *pooled* estimates of yearly abundances. Here, we demonstrate that a spatial version of SPD models can be directly estimated from short time series of spatially referenced distance sampling data in a unified hierarchical state-space modeling framework that also allows for spatial variance (covariance) in population growth. We also show that a full range of likelihood based inference, including estimability diagnostics and model selection, is feasible in this class of models using a data cloning algorithm. We further show through simulation experiments that the hierarchical state-space framework introduced herein efficiently captures the underlying dynamical parameters and spatial abundance distribution. We apply our methodology by analyzing a time series of line-transect distance sampling data for fin whales (*Balaenoptera physalus*) off the U.S. west coast. Although there were only seven surveys conducted during the study time frame, 1991–2014, our analysis detected presence of strong density regulation and provided reliable estimates of fin whale densities. In summary, we show that the integrative framework developed herein allows ecologists to better infer key population characteristics such as presence of density regulation and spatial variability in a population's intrinsic growth potential.

Key words: Akaike information criterion; density dependence; distance sampling; fin whale (Balaenoptera physalus); *Gaussian process; maximum likelihood estimation; model identifiability; nonlinear autoregressive model; Ricker model; spatial modelling; state-space models.*

Introduction

Phenomenological population dynamics models, such as the density-independent diffusion approximation model (Dennis et al. 1991), are powerful for studying long-term dynamics of wildlife populations. However, a fundamental question in understanding the underlying dynamics is whether or not a population is self-regulated, i.e., growth rate is negatively density dependent (Sibly and Hone 2002, Brook and Bradshaw 2006). A suite of stochastic population growth models, such as theta-logistic and Beverton-Holt models (Ponciano et al. 2009, Pedersen et al. 2011) together with well-developed statistical techniques are available to model and test the presence of density dependence (Dennis and Taper 1994, Ponciano et al. 2009). Time series of abundance estimates, such as those arising from mark–recapture or point count surveys, are therefore frequently used to fit these models to study population dynamics and to predict future viability (Dennis and Otten 2000, Dennis et al. 2006). Because available time series are merely estimates of the underlying true abundances, incorporating uncertainty (measurement or observation error) associated with these estimates is an important issue in model estimation and prediction. It is well-established in the recent ecological literature that unaccounted-for observation error can lead to biased estimates of key dynamical parameters and may even mask the form of the underlying growth model (Freckleton et al. 2006, Barker and Sibly 2008, Nadeem and Lele 2012). State-space models, a rich class of general hierarchical models, provide an effective framework for linking the stochastic observation error process to the stochastic population dynamics (or state) process (Pedersen et al. 2011). Fitting these models to time series of abundance estimates yields valid statistical inferences for the biological state process.

Manuscript received 28 July 2015; revised 11 December 2015; accepted 11 January 2016; final version received 15 February 2016. Corresponding Editor: B. E. Kendall.
[3]E-mail: khurram.nadee@gmail.com

In this paper, we show that the conventional state-space approach to fitting stochastic population dynamics (SPD) models to a time series of abundance count data can be extended to modeling spatially referenced distance sampling survey data. Distance sampling methods involve observing animals from a randomly selected set of line or point transects placed within a geographic region (Buckland et al. 2001, Thomas et al. 2010). Distances to animals from the line or point to detections are also measured. In the case of line transects, observers traverse straight lines and measure perpendicular distances of animals from the lines. Assuming that probability of animal detection is a decreasing function of these distances, density estimates can be adjusted for imperfect detection bias (Buckland et al. 2001). An important aspect of distance sampling methods is the spatial replication of line or point transects within the geographic region under study. This, coupled with repeated surveys conducted over a number of years, provides an opportunity to study population dynamics while simultaneously incorporating spatial variability in abundance. Yet most of the existing SPD modeling methods fail to incorporate spatial replicability in such abundance surveys as they employ spatially *pooled* estimates of yearly abundances (e.g., Knape and de Valpine 2012). Here, we demonstrate that SPD models can be estimated from distance sampling data in a unified hierarchical state-space modeling framework that also allows for spatial covariance in population growth.

Incorporating spatial variation in growth and density dependence over a smaller spatial scale has important implications for studying population dynamics and wildlife management (Shima and Osenberg 2003, Johnson 2006, Thorson et al. 2015). Recently, Thorson et al. (2015) conducted a simulation study involving a spatial Gompertz state-space model to investigate the effect of spatial variability in population density. Their analysis showed that the conventional nonspatial Gompertz model (Knape and de Valpine 2012) resulted in markedly biased estimates of density dependence when densities were allowed to vary spatially. However, their spatial Gompertz model provided accurate and precise estimates of density dependence, highlighting the importance of incorporating spatial structure in SPD models.

Our state-space formulation here consists of two model components: (1) a spatial SPD process model and (2) a hierarchical distance sampling (HDS) observation process model. Distance sampling models (which represent the observation process in the current setting) have seen considerable development in the past decade to account for variability in both detection probability and spatial population density (Royle et al. 2004, Johnson et al. 2010, Sillett et al. 2012, Oedekoven et al. 2013). Recently, extending the model presented in Sillett et al. (2012) involving covariate effects on both detection and abundance, Sollmann et al. (2015) developed an open population HDS model to account for temporal variation in abundance from multiple-survey distance sampling data. They employed Dail and Madsen (2011) Markov state process model to model abundance transitions between survey replicates and showed its usefulness in detecting population trends through a simulation study. However, our modeling approach here is novel in a number of ways, e.g.: (1) we replace the simpler Markov process model of Sollmann et al. (2015) with the classical SPD modeling structure (Dennis and Taper 1994, De Valpine and Hastings 2002), thereby allowing estimation of key population parameters quantifying intrinsic growth potential and strength of density regulation, (2) our process model allows for spatial autocorrelation in growth by introducing a parsimonious variance–covariance structure for the spatial environmental noise process, and (3) it allows for population prediction in space and time by exploiting the spatiotemporal correlation structure inherent in the model.

We exemplify our methodology by analyzing a time series of line-transect distance sampling data for a fin whales (*Balaenoptera physalus*) population off the U.S. west coast. Earlier, Moore and Barlow (2011) analysed a part of this same data set to detect population trend using a log-normal process model for $D_{s,t}$ (animal abundance on a unit area in site s, year t) where the mean parameter was modeled as a linear function of time. We analyze the fin whales distance sampling data using data cloning (for details, see Lele et al. 2007, 2010 and Nadeem 2013) to conduct frequentist inference, including likelihood based model estimation, model selection and prediction of process states. We also conduct a simulation study to assess parameter estimation and spatial density prediction using the standard Bayesian Markov chain Monte Carlo (MCMC) framework. Results indicate that the proposed state-space modeling approach is efficient in detecting density regulation even for very short time series data. Our model provides a powerful mechanism in predicting spatial abundance as compared to a non-spatial version of the same process model.

Materials and Methods

Spatial state-space Ricker model

The classical Ricker (1954) state-space model for population time series analysis is given as (Dennis and Taper 1994, De Valpine and Hastings 2002, Dennis et al. 2006):

$$\text{State Process:} \quad X_t = X_{t-1} + a + be^{X_{t-1}} + \varepsilon_t \tag{1-a}$$

$$\text{Observation Process:} \quad W_t | D_t \sim f_W(w_t; D_t, \boldsymbol{\psi}) \tag{1-b}$$

where $X_t = \log D_t$ is the true underlying log-population density at time t, W_t is the corresponding abundance estimate, $\varepsilon_t \sim N(0, \sigma_\varepsilon^2)$ represents environmental noise process and $f_W(.)$ denotes the observation error distribution that may depend on an unknown parameter vector $\boldsymbol{\psi}$. The functional form of the Ricker growth model, $a + be^{X_{t-1}}$, determines the form of density dependent

population dynamics, where the intrinsic growth parameter, a, quantifies growth rate at small abundance levels and density dependent growth occurs when $b < 0$. Assuming that our population of interest consists of S subpopulations defined by their geographic locations, $s = 1,2\ldots,S$; we consider the following spatial version of the Ricker SPD model:

$$X_{s,t} = X_{s,t-1} + a_s + be^{X_{s,t-1}} + \varepsilon_{s,t}, \tag{2-a}$$

$$\varepsilon_t = (\varepsilon_{1,t}, \varepsilon_{2,t}, \ldots, \varepsilon_{S,t})' \sim N(\mathbf{0}, \mathbf{\Sigma}_\varepsilon) \tag{2-b}$$

where ε_t is serially independent environmental noise vector and Σ_ε is spatial variance–covariance matrix accounting for correlation in site-specific population growth, conditional on previous year's log-abundance levels $\mathbf{X}_{t-1} = (X_{1,t-1}, X_{2,t-1}, \ldots, X_{S,t-1})'$. We introduce spatial correlation between sites via an isotropic correlation function $\rho^{d(i,j)}$, where $d(i, j)$ denotes the Euclidean distance between the sites (i, j). The resulting covariance structure is a special case of a Matérn covariance function (Cressie and Wikle 2011). The spatial variance–covariance matrix is then given as

$$\mathbf{\Sigma}_\varepsilon = \sigma^2_\varepsilon \mathrm{R} \tag{3}$$

where $\mathbf{R}$ is a correlation matrix whose (i, j)th entry is defined by $\rho^{d(i,j)}$. This defines the multi-site environmental noise process (2b) as a Gaussian process (see, e.g., Cressie and Wikle 2011). We also need to specify an initial probability distribution for the state process time series $\{\mathbf{X}_t\}_{t=1}^T$ when $t = 1$, i.e., for $\mathbf{X}_1$. Further details on this are included in Appendix S1.

The intrinsic growth rate a, now spatially referenced in Eq. 2, can further be modeled in a number of ways depending on the availability of environmental covariates. For instance, when time series of site-specific abundance covariates are available, we have

$$a_{s,t} = a + \sum_{p=1}^{P_z} \beta_p^{(z)} z_{p,s,t} \tag{4}$$

where $z_{p,s,t}$ is the pth covariate value observed in year t at site s. Alternatively, when covariates only represent habitat suitability not observed temporally, Eq. 4 can be remodeled as

$$a_s = a + \sum_{p=1}^{P_z} \beta_p^{(z)} z_{p,s}. \tag{5}$$

When no environmental covariates are available at all, we can still account for spatial covariability in intrinsic growth rate as

$$\mathbf{a}_s = (a_1, a_2, \ldots, a_S)' \sim N(a\mathbf{1}_S, \mathbf{\Sigma}_a) \tag{6}$$

where $\mathbf{1}_S$ is an S-dimensional vector with all elements as 1 and a is the mean intrinsic growth rate. The spatial variance–covariance matrix $\mathbf{\Sigma}_a$ can be modeled as $\Sigma_a = \sigma_a^2 \boldsymbol{R}$, where $\boldsymbol{R}$ is as defined in Eq. 3. For an example of a similar modeling approach in the context of spatial Gompertz population dynamics model, we refer the reader to Thorson et al. (2015).

Hierarchical distance sampling model

In this section, we describe an HDS model that we employ in our simulation study. Let $N_{s,t}$ denote the animal abundance on a distance sampling effort area of size $\alpha_{s,t}$ surveyed in year t on a given site s. Conditional on $D_{s,t}$, we model the transect abundance $N_{s,t}$ as

$$N_{s,t} | D_{s,t} \sim \text{Poisson}(\lambda_{s,t}); \log \lambda_{s,t} = \log D_{s,t} + \log \alpha_{s,t}. \tag{7}$$

Note that we define $D_{s,t}$ as animal abundance on a unit area in site s, which includes the effort area, $\alpha_{s,t}$, as a subset. Furthermore, unlike Sollmann et al. (2015) who parameterize their Poisson process model directly on population size $N_{s,t}$, we view $N_{s,t}$ as a function of animal density, $D_{s,t}$, where $\log D_{s,t}$ $(=X_{s,t})$ is modeled via the spatial Ricker SPD model (Eq. 2).

Here, for simplicity of exposition, we only consider line transect sampling. Partitioning the transect half-width, ω, into I equi-length distance intervals and conditioning on the latent transect abundance $N_{s,t}$, the vector of animal counts, $\tilde{\mathbf{n}}_{s,t} = (n_{s,t,1}, n_{s,t,2}, \ldots, n_{s,t,I}, N_{s,t} - \sum_{i=1}^I n_{s,t,i})'$, is modeled as a conditional multinomial random vector (Royle et al. 2004):

$$\tilde{\mathbf{n}}_{s,t} | N_{s,t} \sim \text{Multinomial}\left(N_{s,t}, \tilde{\pi}_{s,t}\right) \tag{8}$$

where $\tilde{\pi}_{s,t} = (\pi_{s,t,1}, \pi_{s,t,2}, \ldots, \pi_{s,t,I}, 1 - \pi_{s,t})'$ and $\pi_{s,t} = \sum_{i=1}^I \pi_{s,t,i}$ is the total probability of detection given by an integral of the half-normal detection function, $g(h; \sigma^2)$ (Buckland et al. 2001):

$$\pi_{s,t} = \frac{1}{\omega} \int_0^\omega g(h; \sigma^2_{s,t}) \mathrm{d}h = \frac{1}{\omega} \int_0^\omega \exp\left(-\frac{h^2}{2\sigma^2_{s,t}}\right) \mathrm{d}h.$$

Notice that the modeling framework developed here also allows for other detection functions described in Buckland et al. (2001). When site-specific detection covariates are also available, the scale parameter $\sigma_{s,t}$ can be modeled as (Moore and Barlow 2011, Oedekoven et al. 2013)

$$\log(\sigma_{s,t}) = \beta_0^{(u)} + \sum_{p=1}^{P_u} \beta_p^{(u)} u_{p,s,t}, \tag{9}$$

where $u_{p,s,t}$ is the pth detectability related covariate value observed in year t at site s for $p = 1,2,\ldots,P_u$.

It is conventionally assumed that detection is perfect on the transect line (i.e., at distance $h = 0$), which corresponds to $g(0) = 1$. If detection is imperfect at $h = 0$, a separate estimate of $g(0)$ is required to rescale the

detection function. However, the additional parameter, $g(0)$, is typically inestimable from distance sampling data alone as additional auxiliary information is required for its estimation (e.g., Laake and Borchers 2004, Barlow 2015). We assume $g(0) = 1$ in our simulation study; however, we explicitly account for imperfect detection on the survey trackline in our fin whales case study.

Conditioning on animal density $D_{s,t}$, but marginal on the transect abundance $N_{s,t}$, we can show that joint distribution of observed animal counts, $\mathbf{n}_{s,t} = (n_{s,t,1}, n_{s,t,2}, \ldots, n_{s,t,I})$, is given as (Royle 2004):

$$f_{\mathbf{n}}(\mathbf{n}_{s,t}|D_{s,t}) = \prod_{i=1}^{I} \text{Poisson}(n_{s,t,i}; \lambda_{s,t}\pi_{s,t,i})$$

which is the *observation process* model in the state-space formulation outlined in Eq. 1. The observation model for the full distance sampling data array $\mathbf{n}_{s,t}$, consisting of observed animal counts, can be written as

$$f_{\mathbf{n}}(\mathbf{n}|\boldsymbol{D}) = \prod_{s=1}^{S}\prod_{t=1}^{T}\prod_{i=1}^{I} \text{Poisson}(n_{s,t,i}; \lambda_{s,t}\pi_{s,t,i}) \qquad (10)$$

where $\mathbf{D}$ is the $S \times T$ latent animal density matrix over S sites and T years. Notice that the observation model (Eq. 10) is an instance of a generalized linear mixed model (GLMM) where Poisson counts are modeled via a log-linear link function, i.e.,

$$\log(E(n_{s,t,i}|D_{s,t})) = \log(\alpha_{s,t}) + \log(\pi_{s,t,i}) + X_{s,t}$$

where $X_{s,t}$ (=$\log D_{s,t}$) serves as the spatiotemporal random effect. Further discussion on this and a comparison of the HDS model (Eq. 10) with that of Sollmann et al. (2015) is presented in Appendix S2. Also, a graphical depiction of the various models estimated in this paper is shown in Figs. S1–S3.

Model estimation and selection

No closed form exists for the high dimensional integral appearing in Eq. S8, rendering the maximum likelihood estimation for such non-linear non-Gaussian state-space models computationally intractable. In this paper, we demonstrate how data cloning (DC), a recently developed algorithm for obtaining maximum likelihood estimates (MLEs) and associated standard errors in complex hierarchical models, can be used to conduct likelihood-based inference for models introduced in this paper. We further illustrate that DC is a powerful tool in diagnosing model estimability, a crucial property for valid statistical inference. For further details of the theoretical and computational methodology underlying DC, we refer the reader to Lele et al. (2007, 2010), Sólymos (2010), and Nadeem (2013). We also employ the method developed in Lele et al. (2010) to obtain a likelihood based predictive distribution for the process states, $\mathbf{X}_t$ (see, for detailed illustrations, Nadeem and Lele [2012]).

Although we show that maximum likelihood estimation for analyzing a single real data set is feasible using data cloning, in our simulation study we employed standard Bayesian approach with diffuse prior distributions to contain computational burden. All computations, for both DC and Bayesian inference, were performed using the MCMC samplers implemented in JAGS 3.1.0 (Plummer 2003) via the dclone package (Sólymos 2010) of the R computing software (R Core Team 2014). A summary of prior distributions for respective model parameters is reported in Table S1. We also provide R and JAGS code in Data S1 for the Monte Carlo simulation studies and DC based analysis of the case study model presented in the next section.

As we remarked in the *Introduction*, understanding and quantifying the extent of density regulation in wildlife populations is at the heart of population viability analysis (Dennis and Taper 1994). Here we compute the Akaike information criterion (AIC) index (Burnham and Anderson 2004) to illustrate that presence of density dependence can be detected within the modeling framework presented herein. A key ingredient in hypothesis testing and model selection analyses is the likelihood ratio (LR) statistic. However, computation of LRs is generally intractable in complex hierarchical models as one needs to calculate the maximized value of analytically intractable likelihood functions such as in Eq. S8. Recently, Ponciano et al. (2009) presented a computationally efficient Monte Carlo algorithm for computing LRs in hierarchical models. See Nadeem (2013) for detailed illustrations of its implementation in the context of state-space population dynamics models.

Monte Carlo simulations

We evaluate model performance by simulating 100 distance sampling data sets under the hierarchical state-space model (HSSM) defined by the process model (Eq. 2) and the observation model (Eq. 10). We separately assess estimation performance under the spatial intrinsic growth models defined by Eqs. 4 and 6, where we denote the resulting state-space models as HSSM-I and HSSM-II, respectively (Table S2). We sample the distance-sampling data at 25 sites, where site coordinates are generated from two independent uniform variates. Keeping in view the short time series length of the case study data set (seven survey years), we generate 10- and 6-yr-long distance sampling time series data under HSSM-I and HSSM-II, respectively.

For both models, we simulate population trajectories under stationary population dynamics with process growth model parameters set to $(a, b, \sigma_e^2) = (1.00, -0.01, 1.00)$. To subject our modeling approach to a stricter evaluation, we do not consider other dynamical scenarios, such as recovering populations and/or larger environmental noise, as the Ricker

growth model parameters are shown to be estimable with high accuracy under these scenarios (Dennis and Taper 1994). For simplicity of exposition, we assume a single covariate both in the intrinsic growth model (Eq. 4) and the detection model (Eq. 9). These covariates, $z_{s,t}$ and $u_{s,t}$, are independently generated from zero-mean Gaussian distributions with variances 0.1 and 1.0 respectively. True values of all the model parameters are reported in Table S2.

It is important to note that the Ricker growth model generates chaotic population dynamics for $a > 3.0$ (Turchin 2003), making it highly intractable for statistical inference in the state-space framework using standard estimation techniques (Wood 2010). We therefore chose parameter values in Eqs. 4 and 6 such that the resulting simulated intrinsic growth effects ($a_{s,t}$ and a_s under HSSM-I and HSSM-II, respectively) remain less than 2.0 in all simulations. Value of the spatial correlation parameter ρ (Table S2) is chosen such that it gives a correlation of 0.25 between two sites located on the diagonal vertices of the unit square.

For simulations under HSSM-II, we consider the scenario where some of the sites are not visited after the first survey year, resulting in missing surveys in years 2–6 for such sites. Specifically, we randomly selected five *unsurveyed* sites from the total 25 sites. However, selection of such sites can be based on logistical convenience and geographic location in real distance sampling applications. We show that the animal density on these unsurveyed sites is accurately predicted by exploiting the underlying spatial correlation structure in population growth. This strategy can be repeated in the subsequent five years ($t = 6, 7, \ldots, 10$) by selecting a different set of unsurveyed sites while resuming surveys on the earlier skipped sites. We also fit the model under the hypothesis that $\rho = 0$, to show that density estimation is significantly biased (see *Results*) when spatial correlation between sites is ignored.

Convergence of MCMC chains in HSSM-I simulation study and fin whales case study was satisfactory. However, for the HSSM-II simulation study, we found poor convergence in our simulation studies for the latent log-abundance in the unsurveyed sites, $\mathbf{X}_t^{(U)} = (X_{21,t}, X_{22,t}, \ldots X_{25,t})$. To address this issue, we provide a simple algorithm to compute a predictive posterior distribution of $\mathbf{X}_t^{(U)}$, whose details are given in Appendix S3.

Fin whales case study

Under the U.S. Marine Mammal Protection Act, population assessments must be conducted for marine mammal stocks inhabiting U.S. waters. Marine Mammal Stock Assessment Reports (e.g., Carretta et al. 2014) include estimates of animal abundance and population trends within the U.S. Exclusive Economic Zone, which encompasses only a fraction of most populations. The Southwest Fisheries Science Center, part of the National Marine Fisheries Service, systematically conducted seven ship-based line-transect surveys for cetaceans in waters off the U.S. west coast during late summer and autumn between 1991 and 2014. Data through 2008 (the first six surveys) have been used to estimate abundance trends for fin whales (*B. physalus*), beaked whales (family Ziphiidae), and sperm whales (*Physeter macrocephalus*) from a simpler hierarchical distance sampling model (exponential growth process model, no spatial covariance in the observation model) (Moore and Barlow 2011, 2013, 2014). The current analysis provides updated abundance and trend estimates for fin whales based on the newer model, new estimates of $g(0)$, and inclusion of the 2014 survey data.

Refer to Barlow and Forney (2007) and Moore and Barlow (2011) for details of the survey design, field methods, and description of the fin whale and effort data through 2008. Of particular relevance to the current analysis is that the study area is divided into four strata of roughly similar size from north to south: Oregon–Washington, Northern California, Central California, and Southern California. For the 2014 survey, stratum effort was, from north to south: 2706, 1998, 1839, 2779 km (total: 9322 km). Only sightings ≤5.5 km from the vessel are included for the current analysis (in the earlier analysis by Moore and Barlow 2011, only sightings within 4 km were used). In 2014, there were 32, 36, 20, and 8 group sightings per stratum (from north to south; total = 96). Mean group size for fin whales across the entire data set is approximately two animals. Many covariates potentially affecting sighting probability are recorded along the effort transects. In general across cetacean species, the most important is Beaufort sea state, recorded as an integer ranging from 0 (no wind, sea like a mirror) through 5 (~20-knot winds with many waves and white caps). Our analysis here is restricted to the impact of this variable on group detection rates.

Let us now present the modeling framework for the fin whale data set. Unlike the simulation study where our response variable was number of animals detected within the effort area partitioned in I distance intervals, here we have the actual detection distances available as well. Let us first introduce some notation (where all distance units are in kilometers):

j, Beaufort state with possible values 1, 2, …, 5 (0 and 1 are combined in integer value 1);
$L_{s,t,j}$, total transect length (km) in year t in stratum s with Beaufort state j;
$\alpha_{s,t,j}$, effort area corresponding to $L_{s,t,j}$, given as $\alpha_{s,t,j} = 2\omega L_{s,t,j}$, where ω is the transect half-width, i.e., 5.5 km;
$n_{s,t,j}$, number of fin whale groups detected within $\alpha_{s,t,j}$;
$y_{s,t,j,k}$, distance of the kth detection made within effort area $\alpha_{s,t,j}$ (see Moore and Barlow 2011, for example frequency distributions of fin whale detection distances);
$g_j(0)$, probability of detection on the transect line with Beaufort state j;
φ_t, mean fin whale group size in year t;

$W_t = \sum_{s=1}^{4} D_{s,t} A_s$, total animal abundance within the whole study area, where A_s is the area (km^2) of the sth survey stratum with corresponding abundance in year t given as $D_{s,t} A_s$.

The full observation model is then given as follows:

$$Y_{s,t,j,k} \sim f_H\left(y_{s,t,j,k}; \sigma^2_{s,t,j}\right) \tag{11}$$

where $f_H(.)$ is the half-normal distribution, truncated at $\omega = 5.5$ km; and

$$\log(\sigma_{s,t,j}) = \beta_0 + j\beta_{\text{beaufort}} \tag{12}$$

$$n_{s,t,j} | D_{s,t} \sim \text{Poisson}\left(\lambda^{(n)}_{s,t,j}\right) \tag{13}$$

$$\lambda^{(n)}_{s,t,j} = \frac{\alpha_{s,t,j} g_j(0) \pi_{s,t,j} D_{s,t}}{\phi_t} \quad \text{where} \quad \pi_{s,t,j} = \frac{1}{\omega}\int_0^{\omega} \exp\left(-\frac{h^2}{2\sigma^2_{s,t,j}}\right) \mathrm{d}h.$$

Barlow (2015) derived estimates of $g_j(0)$ using a model-based approach only involving fin-whale detections on the trackline in varying survey conditions. The model form is given as

$$g_j(0) = g_1(0) e^{j\beta_{g0}} \quad \text{where} \quad j > 1. \tag{14}$$

Importantly, these newer Beaufort-dependent $g(0)$ estimates provide for a much lower marginal $g_1(0)$ estimate than the constant estimate of $g_j(0) = 0.92$ used by Moore and Barlow (2011), so the new density and abundance estimates are expected to be considerably higher. Here we use the estimate of $g_1(0) = 0.92$ for Beaufort states 0 and 1 ($j = 1$) and then calculate $g_j(0)$ for higher sea states based on the estimate of β_{g0} obtained in Barlow (2015). However, we only incorporate uncertainty associated with the $g_1(0) = 0.92$ estimate reported in Barlow and Forney (2007).

As no abundance-related covariates are available, and because we only have a small number of strata (sites), we assume stratum-specific intrinsic growth rate effects, (a_1, a_2, a_3, a_4) as unknown parameters in the process model (Eq. 2). We separately estimate mean group size φ_t from the observed fin whale group sizes, with details provided in Appendix S4, where we report a simple algorithm for incorporating the uncertainty in the estimates of (φ_t, $g_1(0)$) in our DC-based maximum likelihood estimation.

Results

Monte Carlo simulation study

Table S2 summarizes Bayesian estimation of model parameters from analyzing simulated distance sampling data generated under HSSM-I and HSSM-II, respectively. Summary statistics for bias and root mean square error (RMSE) of the parameter estimates indicate that observation model parameters ($\beta_0^{(u)}$,$\beta_1^{(u)}$) are estimated accurately under both models. The coefficient of the habitat related environmental covariate, ($\beta_1^{(z)}$), in HSSM-I is also accurately estimable. Estimation of the underlying intrinsic growth parameter, a, and the density dependent parameter, b, is also unbiased under both models. However, estimation of the population carrying capacity, $K = -a/b$, is slightly biased downwards under HSSM_II. Note that here K is, in a sense, an *average* carrying capacity over the entire study region as it is computed via the underlying single intrinsic growth parameter a. Parameters (ρ, σ_ε) associated with the environmental noise variance-covariance matrix, $\Sigma\varepsilon$, are slightly biased downwards under HSSM-I. However, there is considerable upward bias under HSSM-II, likely resulting from strong interaction among the variance–covariance related parameters (ρ,σ_ε,σ_a,σ_{X_1}) in HSSM-II.

The RMSE values are generally larger under HSSM-II, consistent with the facts that (1) we have smaller number of sites and years (20 and 6, respectively) as compared to those employed for HSSM-I (25 sites and 10 years), and (2) unlike HSSM-I, HSSM-II does not include habitat related covariate information in the spatial intrinsic growth model. Notice that the RMSE of K is much larger under HSSM-II as compared to that of under HSSM-I. This is because the spatiotemporal variability in intrinsic growth under HSSM-I is effectively explained by the observed habitat covariate, $z_{s,t}$. On the other hand, absence of such a covariate in HSSM-II results in higher uncertainty in predicting site-specific intrinsic growth rate effects a_s, which in turn induces large uncertainty in estimation of K.

Next we assess model performance in predicting the underlying spatial (log-) abundance densities (Fig. 1). It is evident that site-specific abundance prediction under HSSM-I is unbiased with good precision (Fig. 1a; RMSE = 0.1751). Fig. 1b depicts predictive accuracy under HSSM-II for the five unsurveyed sites over five survey years, from year 2 to 6. We also compare the performance by fitting a simpler model that ignores spatial correlation in the environmental noise process, ($\rho = \sigma_a = 0$; gray points in Fig. 1b). This without-spatial-correlation model seems to accurately predict densities only near the carrying capacity $K = 100$. However, as the true densities fluctuate away from the carrying capacity, the accuracy deteriorates as predictions are significantly biased upward and downward whenever the true densities move above and below the carrying capacity threshold (RMSE = 0.3799). The predictive performance under HSSM-II is however unaffected by the underlying stochastic fluctuations in population abundance, and is much superior as compared to the simpler without-spatial-correlation model (RMSE = 0.1942). Thus, the spatial correlation structure inherent in HSSM-II helps accurately predict abundance densities around the unsurveyed sites.

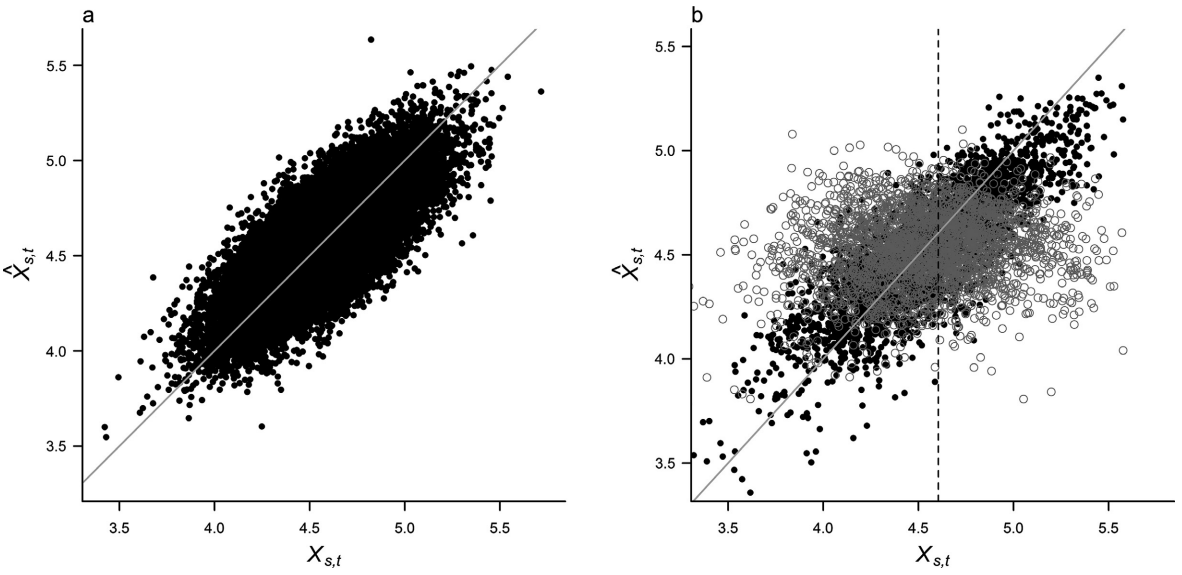

FIG. 1. (a) True ($X_{s,t}$) vs. predicted ($\hat{X}_{s,t}$) log-abundance densities under HSSM-I and (b) the same under HSSM-II (black points) and nonspatial HSSM-II ($\rho = \sigma_a = 0$, gray points) across 100 simulated data sets. Predictions shown under HSSM-II are for the five unsurveyed sites during years 2–6. Gray lines indicate ideal predictive performance (RMSE = 0) and the vertical dashed line marks the log-transformed carrying capacity level (log K).

Fin whales case study

Table 1 summarizes maximum likelihood estimates and associated asymptotic standard errors for various model parameters for the fin whale data set, where we use $\beta_{g0} = -0.2718$ estimate from Barlow (2015). We fit the original model as described by Eqs. 11–14 (also see Fig. S3), including parameters β_{beaufort} for the effect of Beaufort sea state on the detection function parameter $\sigma_{s,t,j}$ as well as β_{g0} for sea-state-dependent $g_j(0)$ (Eq. 14). However, there was no evidence for a sea-state effect on the detection function, as the estimate of β_{beaufort}, which is expected to be negative if sea state matters, was slightly positive with a Wald-type confidence interval (CI) substantially overlapping zero ($\hat{\beta}_{\text{beaufort}} = 0.0325$; CI: −0.0424, 0.1074). Note that Moore and Barlow (2011) also did not find evidence for an effect of sea state on the fin whale detection function. Therefore, Table 1 presents revised model estimates with β_{beaufort} excluded (Model H_1).

Our DC-based estimability diagnostics indicated that all the model parameters in the original model, including (β_{g0}, β_{beaufort}) are directly estimable from fin whales distance sampling data (Table S4). This is surprising at first glance; however, as the graphical depiction in Fig. S3 indicates, parameters (β_0, β_{beaufort}) are estimable in Eqs. 11–12 from the observed distance measurements, $y_{s,t,j,k}$, alone. Therefore, there is sufficient information available in the observed fin whale counts, $n_{s,t,j}$, to render β_{g0} as separately estimable (see Eq. 13). The estimate of β_{g0} obtained directly from distance sampling data under H_1 is −0.1729 (Table S4), indicating that detectability on the trackline deteriorates as sea conditions become rougher. However, this estimate is considerably less negative than the coefficient approximating Barlow's (2015) β_{g0} estimate (−0.2718). Barlow (2015) obtained his estimate using a spatial model for animal density, whereas our model here only estimates stratum differences in density. Direct estimation of β_{g0} (Table S4) may be confounded with animal

TABLE 1. Maximum likelihood estimates of parameters in the hierarchical state-space models fitted to the fin whale (*Balaenoptera physalus*) distance sampling data, where we use $\beta_{g0} = -0.2718$ estimate from Barlow (2015).

Model	a_1	a_2	a_3	a_4	b	β_0	σ_ε	ρ	ΔAIC
H_1	0.1691 (0.0805)	0.4253 (0.1689)	0.4320 (0.1252)	0.3077 (0.1043)	−0.0009 (0.0004)	0.9296 (0.0501)	0.2402 (0.0874)	0.0357 (0.0891)	0
H_{0a}	0.2265† (0.0840)	–	–	–	−0.0006 (0.0003)	0.9302 (0.0477)	0.3124 (0.0940)	0.0096 (0.0310)	8.8722
H_{0b}	0.0263 (0.0432)	0.0228 (0.0420)	0.1187 (0.0436)	0.0935 (0.0514)	–	0.9301 (0.0491)	0.1920 (0.0947)	0.0188 (0.0617)	14.5755

Notes: The estimate of b under H_{0a} and H_{0b} also reflects unit area for $D_{s,t}$, which is 50,000 km^2 in all the fitted models. SE appear in parentheses.

†Estimate of a under H_{0a}: $a_1 = a_2 = a_3 = a_4 = a$.

density (e.g., if fin whales are more abundant in rougher more offshore waters, which is at least partly the case). For this reason, we use Barlow's (2015) estimate of $\beta_{g0} = -0.2718$ for the analysis results reported in Table 1. But for comparison and future reference, we also report results corresponding to the distance sampling data-based estimate of β_{g0} (−0.1729) in Tables S4 and S5.

We employed the AIC computation algorithm by Ponciano et al. (2009) for model selection to test two additional biological hypothesis of interest: (1) H_{0a}: $a_1 = a_2 = a_3 = a_4 = a$, and (2) H_{0b}: $s = 0$, which indicates density independent population growth. The corresponding ΔAIC values are reported in Table 1 where Model H_1 attains the lowest AIC value. The large ΔAIC values corresponding to the other two models (H_{0a}, H_{0b}) strongly support the hypothesis that fin whale population growth is density regulated and that the different strata support different intrinsic growth potential.

The a parameters suggest annual population growth rates on the order of 20–50% for a small-population condition (i.e., when growth is not resource-limited). These estimates are likely driven by rapid increases in abundance between the first two surveys (abundance roughly doubled in 3 years; Fig. 2). However, most baleen whale populations cannot increase by more than ≈5–12% annually (depending on the species) from birth and death processes (e.g., Best 1993, Zerbini et al. 2010). Rather, the initial abundance increases were presumably driven by immigration from outside the survey area, which encompasses only part of this fin whale stock. As such, the observed distance sampling data lack information about true intrinsic growth potential for fin whales owing to the several missing survey years throughout the study period. However, the estimates of annual rate of change within the survey time frame, given by the combination of a and b, $a+be^{X_{t-1}}$ (see 1-a), were reasonable and qualitatively comparable to those estimated by Moore and Barlow (2011). The geometric mean for yearly growth rates, N_t/N_{t-1}, from 1991 to 2014 had a mean of 1.075 (95% prediction interval based on predictive process distributions: 1.051–1.098). The strongest increases in abundance occurred after the 1991 survey and again between the 2001 and 2005 surveys (Fig. 2b). Total abundance in 2014 was similar to 2008, though this varied by stratum. In the 1990s, population density was highest by far in the Central California stratum (Fig 2a). This has remained an area of high (though not consistently increasing) density for fin whales. Densities have become similarly high in Northern California and off Oregon-Washington following strong and steady increases in these areas since the earliest surveys. Fin whale density in Southern California has been lower than in the other strata since 2001 and generally non-trending (but variable) since 1996. In all, there has been a roughly five-fold increase in fin whale abundance within the California Current study area between 1991 and 2014.

The spatial Ricker process model indicated weak spatial correlation between the adjacent strata (mean $\rho^{d(i,j)} = 0.319$), which further declined for the non-adjacent strata ($\rho^{d(i,j)} = 0.036$ for Southern California and Oregon–Washington, the two outermost strata). As our simulation study for the HSSM-II suggested, presence of spatial correlation was useful for predicting fin whale density in Oregon–Washington during the years 1991 and 1993 (Fig. 2a; recall this stratum was not surveyed in these two years).

Notice that abundance estimates are much higher for this analysis (Fig. 2b) than those of Moore and Barlow (2011) because of the new $g(0)$ model component (Eq. 14)

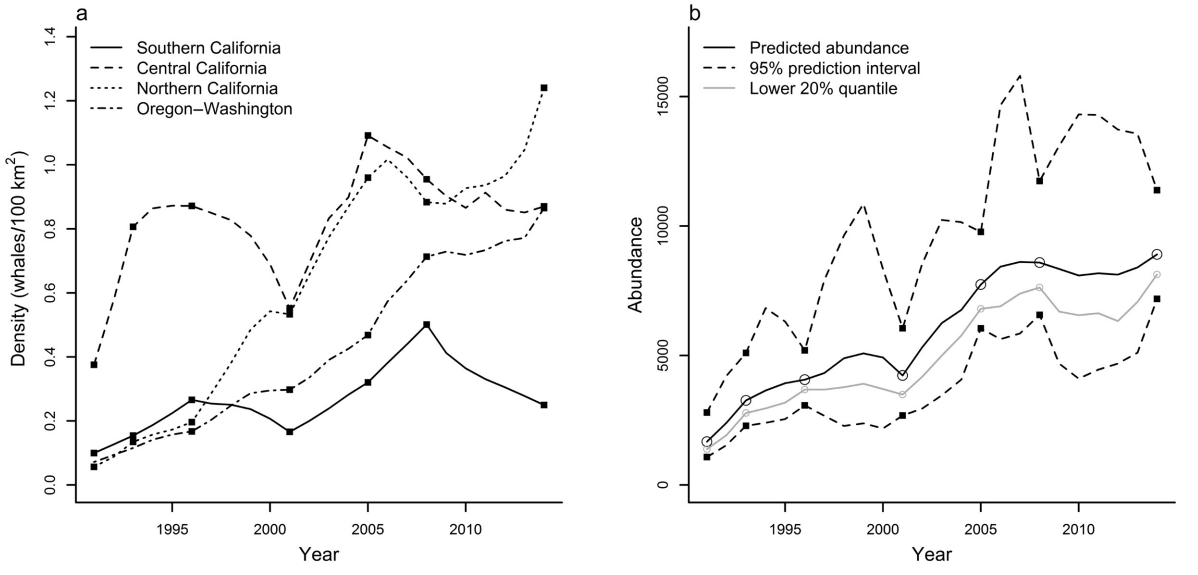

FIG. 2. (a) Predicted fin whale density (whales/100 km²) by year and stratum. (b) Predicted total abundance along with 95% prediction intervals and the lower 20% quantile of the respective predictive distributions. Note that the Oregon–Washington stratum was not surveyed in 1991 and 1993. Different symbols (circles, squares) in both panels indicate the survey years: 1991, 1993, 1996, 2001, 2005, 2008, and 2014.

introduced here. For the four survey years between 1996 and 2008, abundance predictions ranged from 2.0 to 2.9 times higher in the new analysis. A complete summary of abundance estimates are in Table S3; these include outputs relevant to the fin whale stock assessment report required under the U.S. Marine Mammal Protection Act.

Discussion

Distance sampling methods are widespread in monitoring wildlife populations. (Buckland et al. 2001, Royle 2004, Thomas et al. 2010). Recent developments in model-based distance sampling methods, such as incorporation of spatial heterogeneity in abundance and detection probability as a function of observable covariates, have resulted in improved estimation of abundance over large geographic scales (Marques et al. 2007, Sillett et al. 2012, Oedekoven et al. 2013). Time series of distance sampling data presents additional opportunity to study population trends and temporal dynamics in population growth using phenomenological population growth models (Dennis et al. 1991). A naïve approach to such an analysis is to fit population growth models to individual abundance estimates obtained from distance sampling analyses (see, for instance, Jolles 2007). But uncertainty is often mishandled when taking this approach, which can result in unreliable model estimation and mislead wildlife conservation management (Freckleton et al. 2006, Nadeem and Lele 2012). Improved frameworks have been developed (e.g., Moore and Barlow 2011, 2013, 2014); but we have taken this work further by developing a comprehensive state-space modeling approach that integrates distance sampling with a spatially explicit population process. By incorporating spatial variability in population growth within a unified framework (inference on SPD process model and the distance sampling observation model obtained simultaneously), ecologists can better infer key population characteristics such as presence of density regulation and spatial variability in a population's intrinsic growth potential.

Our modeling framework is analytically more tractable compared to the generalized Markov model of Sollmann et al. (2015), which they introduced in order to take into account recolonization from the neighboring sites as their simpler log-linear trend model performed poorly when fitted to simulated data generated with recolonization allowed. Specifically, we show in Appendix S2 that the true population rate of change under the generalized Markov model is given as $\tilde{\gamma} = \gamma + \exp(\tau^2/2)/N_{s,t-1}$, where γ is the population rate of change that can be thought of as the sum of survival probability φ and recruitment rate ν; and τ^2 is an immigration process related variance parameter. However, as Sollmann et al. (2015) remark, this rate of change is inestimable because γ and τ^2 are confounded. A similar population rate of change can be computed under our formulation (see Appendix S2 for details), given as $\gamma_{\text{HSSM}} = \alpha_{s,t} \exp(a + bD_{s,t-1} + \sigma_\varepsilon^2/2)$ where $\alpha_{s,t}$ is the distance sampling effort area. Here, γ_{HSSM} is estimable because the underlying state-process parameters $(a,b,\sigma_\varepsilon^2)$ are all separately estimable. We further note that the Ricker SPD model (Eq. 2) accounts for the dependence of $D_{s,t}$ on $D_{s,t-1}$; hence, implicitly that of $N_{s,t}$ on $D_{s,t-1}$ via Eq. 7, whereas any net immigration effect is implicitly explained by the variance–covariance parameters $(\sigma_\varepsilon^2,\rho)$. Therefore, relocation is automatically incorporated within our modeling framework. Given that the parameters under the HDS model (Eq. 10) and process model (Eq. 2) are all estimable, the modeling framework developed herein is much more useful from a statistical analysis viewpoint since it allows, for example, quantification of density dependence and estimation of site-specific abundances.

In the case of fin whales occupying the California Current study area, our approach provided improved estimates of abundance (especially for the less-surveyed Oregon–Washington stratum) and population trend, with abundance coefficient of variations (CVs) that were smaller (Table S3) than those provided by Moore and Barlow (2011) even though we incorporated a new source of uncertainty in the present analysis (i.e., to account for the relationship between Beaufort sea state and $g(0)$). The recent realization that $g(0)$ varies with sea state (Barlow 2015) has important consequences for marine mammal population estimates and management; our fin whale estimates here are more than double the previous estimates. Our DC based analysis framework elegantly accounts for this relationship, and if a spatial model for animal density were incorporated in the analysis, then $\beta_{g(0)}$ in Eq. 14 is estimable from the distance sampling data directly, thereby obviating the reliance on external estimates of relative $g(0)$ values.

Likelihood based inference for the class of non-linear non-Gaussian state-space models is highly intractable even for univariate time series processes (De Valpine 2002, Kantas et al. 2015). The form of the observation process model, $f_W(.)$, in the standard setting is also simple, e.g., a Gaussian or Poisson model with at most one unknown parameter (De Valpine 2002, Pedersen et al. 2011). The nonlinear state-space framework considered here adds further complexity in that it replaces the univariate Markov transition density function (Eq. 1a) with a multivariate counterpart (Eq. 2), and instead of using abundance estimates in a simpler observation model, it invokes a full nonlinear hierarchical structure that directly models the observation process, thereby leading to an integrated state-space approach. This allows automatic incorporation of uncertainty associated with abundance estimation in estimating process level parameters. Here we have shown that the full range of likelihood-based inference, including parameter estimation, model estimability, model selection, and prediction of process states, is computationally accessible within this extended class of state-space models using the DC algorithm. Although, we focused on distance sampling observation models only, an important future direction would be to further extend our framework to other observation

process scenarios, e.g., spatial mark–recapture (Royle et al. 2009, Ford et al. 2012) and spatial count models (Hostetler and Chandler 2014).

Recently, Thorson et al. (2015) adapted the stochastic Gompertz model (Dennis and Taper 1994) in Eq. 2 to evaluate density dependence over continuous space within a state-space framework. The linearity in the Gompertz growth model, coupled with the spatial variance-covariance structure as defined in Eq. 3, allowed their process model for $\mathbf{X}_t$ to be a Gaussian random field. The choice of the Gompertz growth form was based on tractable statistical properties of the resulting linear autoregressive SPD model (Dennis and Taper 1994, Thorson et al. 2015). However, the Gompertz model is biologically implausible for densities fluctuating away from the equilibrium state (Ives et al. 2003). In comparison, the Ricker model adapted herein leads to a more biologically rich nonlinear autoregressive process model for $\mathbf{X}_t$, which, conditional on $\mathbf{X}_{t-1}$, also defines a Gaussian random field process in Eq. 2.

Understanding animal movement patterns is also crucial for proper characterization of the variance–covariance structure in spatial SPD models (Morales et al. 2010). The isotropic correlation function used in our analysis allows only for positive correlation in population growth arising, for instance, from synchronous variability in habitat related factors in neighboring sites. However, animal movement on a large geographical scale can induce negative spatial correlation in growth. For instance, negative correlation in fin whale stratum–abundances can occur via shifts in cetacean–habitat configuration due to oceanographic dynamics over large scales, whereby animals move from one stratum to another (Becker et al. 2014). This may explain the declines observed in Southern and Central California density between 2008 and 2014, and concurrent increases of Northern California, Oregon and Washington, as a northward shift in food availability may have driven large scale northward shifts in distribution (Fig. 2a).

Recently, there has been promising progress in development of stochastic animal movement models (see, for instance, Albertsen et al. 2015). We believe that further integrating movement data and models into the HSSM framework developed herein would be a significant contribution, leading to improved insights into population dynamics and distribution in future applications.

Acknowledgments

This research was funded by a postdoctoral fellowship award from the Canadian Statistical Sciences Institute (CANSSI). We thank Jay Barlow and Tim Gerrodette for important discussions and insightful comments. We are also grateful to the associate editor and two anonymous referees for their helpful suggestions in revising an earlier draft.

Literature Cited

Albertsen, C. M., K. Whoriskey, D. Yurkowski, A. Nielsen, and J. Mills Flemming. 2015. Fast fitting of non-Gaussian state-space models to animal movement data via Template Model Builder. Ecology 96:2598–2604.

Barker, D., and R. M. Sibly. 2008. The effects of environmental perturbation and measurement error on estimates of the shape parameter in the theta-logistic model of population regulation. Ecological Modelling 219:170–177.

Barlow, J. 2015. Inferring trackline detection probabilities, g(0), for cetaceans from apparent densities in different survey conditions. Marine Mammal Science 31:923–943.

Barlow, J., and K. A. Forney. 2007. Abundance and population density of cetaceans in the California Current ecosystem. Fishery Bulletin 105:509–526.

Becker, E. A., K. A. Forney, D. G. Foley, R. C. Smith, T. J. Moore, and J. Barlow. 2014. Predicting seasonal density patterns of California cetaceans based on habitat models. Endangered Species Research 23:1–22.

Best, P. B. 1993. Increase rates in severely depleted stocks of baleen whales. ICES Journal of Marine Science: Journal du Conseil 50:169–186.

Brook, B. W., and C. J. A. Bradshaw. 2006. Strength of evidence for density dependence in abundance time series of 1198 species. Ecology 87:1445–1451.

Buckland, S. T., D. R. Anderson, K. P. Burnham, J. L. Laake, and D. L. Borchers. 2001. Introduction to distance sampling: estimating abundance of biological populations. Oxford University Press, Oxford, UK.

Burnham, K. P., and D. R. Anderson. 2004. Multimodel inference understanding AIC and BIC in model selection. Sociological Methods & Research 33:261–304.

Carretta, J.V., et al. 2014. U.S. Pacific marine mammal stock assessments, 2013. NOAA Technical Memorandum. NOAA-TM-NMFS-SWFSC-532. NOAA National Marine Fisheries Service, Silver Spring, Maryland, USA.

Cressie, N., and C. K. Wikle. 2011. Statistics for spatio-temporal data. John Wiley & Sons, Hoboken, New Jersey, USA.

Dail, D., and L. Madsen. 2011. Models for estimating abundance from repeated counts of an open metapopulation. Biometrics 67:577–587.

Dennis, B., and M. R. M. Otten. 2000. Joint effects of density dependence and rainfall on abundance of San Joaquin kit fox. Journal of Wildlife Management 64:388–400.

Dennis, B., and M. L. Taper. 1994. Density dependence in time series observations of natural populations: estimation and testing. Ecological Monographs 64:205–224.

Dennis, B., P. L. Munholland, and J. M. Scott. 1991. Estimation of growth and extinction parameters for endangered species. Ecological Monographs 61:115–143.

Dennis, B., J. M. Ponciano, S. R. Lele, M. L. Taper, and D. F. Staples. 2006. Estimating density dependence, process noise, and observation error. Ecological Monographs 76:323–341.

de Valpine, P. 2002. Review of methods for fitting time-series models with process and observation error and likelihood calculations for nonlinear, non-Gaussian state-space models. Bulletin of Marine Science 70:455–471.

de Valpine, P., and A. Hastings. 2002. Fitting population models incorporating process noise and observation error. Ecological Monographs 72:57–76.

Ford, J. H., M. V. Bravington, and J. Robbins. 2012. Incorporating individual variability into mark–recapture models. Methods in Ecology and Evolution 3:1047–1054.

Freckleton, R. P., A. R. Watkinson, R. E. Green, and W. J. Sutherland. 2006. Census error and the detection of density dependence. Journal of Animal Ecology 75:837–851.

Hostetler, J. A., and R. B. Chandler. 2014. Improved state-space models for inference about spatial and temporal variation in abundance from count data. Ecology 96:1713–1723.

Ives, A. R., B. Dennis, K. L. Cottingham, and S. R. Carpenter. 2003. Estimating community stability and ecological interactions from time-series data. Ecological Monographs 73:301–330.

Johnson, D. W. 2006. Density dependence in marine fish populations revealed at small and large spatial scales. Ecology 87:319–325.

Johnson, D. S., J. L. Laake, and J. M. Ver Hoef. 2010. A model-based approach for making ecological inference from distance sampling data. Biometrics 66:310–318.

Jolles, A. E. 2007. Population biology of African buffalo (*Syncerus caffer*) at Hluhluwe-iMfolozi Park, South Africa. African Journal of Ecology 45:398–406.

Kantas, N., A. Doucet, S. S. Singh, J. M. Maciejowski, and N. Chopin. 2015. On particle methods for parameter estimation in state-space models. arXiv:1412.8695 [stat].

Knape, J., and P. de Valpine. 2012. Are patterns of density dependence in the Global Population Dynamics Database driven by uncertainty about population abundance? Ecology Letters 15:17–23.

Laake, J., and D. Borchers. 2004. Methods for incomplete detection at distance zero. Pages 108–189 *in* S. Buckland, D. Anderson, K. Burnham, J. Laake, D. Borchers, and L. Thomas, editors. Advanced distance sampling. Oxford University Press, Oxford, UK.

Lele, S. R., B. Dennis, and F. Lutscher. 2007. Data cloning: easy maximum likelihood estimation for complex ecological models using Bayesian Markov chain Monte Carlo methods. Ecology Letters 10:551–563.

Lele, S. R., K. Nadeem, and B. Schmuland. 2010. Estimability and likelihood inference for generalized linear mixed models using data cloning. Journal of the American Statistical Association 105:1617–1625.

Marques, T. A., L. Thomas, S. G. Fancy, S. T. Buckland, and C. M. Handel. 2007. Improving estimates of bird density using multiple-covariate distance sampling. Auk 124:1229–1243.

Moore, J. E., and J. P. Barlow. 2011. Bayesian state-space model of fin whale abundance trends from a 1991–2008 time series of line-transect surveys in the California Current. Journal of Applied Ecology 48:1195–1205.

Moore, J. E., and J. P. Barlow. 2013. Declining abundance of beaked whales (family ziphiidae) in the California current large marine ecosystem. PLoS ONE 8:e52770.

Moore, J. E., and J. P. Barlow. 2014. Improved abundance and trend estimates for sperm whales in the eastern North Pacific from Bayesian hierarchical modeling. Endangered Species Research 25:141–150.

Morales, J. M., P. R. Moorcroft, J. Matthiopoulos, J. L. Frair, J. G. Kie, R. A. Powell, E. H. Merrill, and D. T. Haydon. 2010. Building the bridge between animal movement and population dynamics. Philosophical Transactions of the Royal Society B 365:2289–2301.

Nadeem, K. 2013. Estimability and likelihood inference for general hierarchical models using data cloning. Thesis. University of Alberta, Edmonton, Alberta, Canada.

Nadeem, K., and S. R. Lele. 2012. Likelihood based population viability analysis in the presence of observation error. Oikos 121:1656–1664.

Oedekoven, C. S., S. T. Buckland, M. L. Mackenzie, K. O. Evans, and L. W. Burger. 2013. Improving distance sampling: accounting for covariates and non-independency between sampled sites. Journal of Applied Ecology 50:786–793.

Pedersen, M. W., C. W. Berg, U. H. Thygesen, A. Nielsen, and H. Madsen. 2011. Estimation methods for nonlinear state-space models in ecology. Ecological Modelling 222:1394–1400.

Plummer, M. 2003. JAGS: A program for analysis of Bayesian graphical models using Gibbs sampling. Pages 20–22 *in* K. Horik, F. Leisch, and A. Zeilis, editors. Proceedings of the 3rd international workshop on distributed statistical computing (DSC 2003). Vienna, Austria.

Ponciano, J. M., M. L. Taper, B. Dennis, and S. R. Lele. 2009. Hierarchical models in ecology: confidence intervals, hypothesis testing, and model selection using data cloning. Ecology 90:356–362.

R Core Team. 2014. R: A language and environment for statistical computing. R Foundation for Statistical Computing, Vienna, Austria. http://www.R-project.org/.

Ricker, W. E. 1954. Stock and recruitment. Journal of Fisheries Board of Canada 11:559–623.

Royle, J. A. 2004. N-mixture models for estimating population size from spatially replicated counts. Biometrics 60:108–115.

Royle, J. A., D. K. Dawson, and S. Bates. 2004. Modeling abundance effects in distance sampling. Ecology 85:1591–1597.

Royle, J. A., K. U. Karanth, A. M. Gopalaswamy, and N. S. Kumar. 2009. Bayesian inference in camera trapping studies for a class of spatial capture–recapture models. Ecology 90:3233–3244.

Shima, J. S., and C. W. Osenberg. 2003. Cryptic density dependence: effects of covariation between density and site quality in reef fish. Ecology 84:46–52.

Sibly, R. M., and J. Hone. 2002. Population growth rate and its determinants: an overview. Philosophical Transactions of the Royal Society B 357:1153–1170.

Sillett, T. S., R. B. Chandler, J. A. Royle, M. Kéry, and S. A. Morrison. 2012. Hierarchical distance-sampling models to estimate population size and habitat-specific abundance of an island endemic. Ecological Applications 22:1997–2006.

Sollmann, R., B. Gardner, R. B. Chandler, J. A. Royle, and T. S. Sillett. 2015. An open-population hierarchical distance sampling model. Ecology 96:325–331.

Sólymos, P. 2010. dclone: data cloning in R. R Journal 2:29–37.

Thomas, L., S. T. Buckland, E. A. Rexstad, J. L. Laake, S. Strindberg, S. L. Hedley, J. R. B. Bishop, T. A. Marques, and K. P. Burnham. 2010. Distance software: design and analysis of distance sampling surveys for estimating population size. Journal of Applied Ecology 47:5–14.

Thorson, J. T., H. J. Skaug, K. Kristensen, A. O. Shelton, E. J. Ward, J. H. Harms, and J. A. Benante. 2015. The importance of spatial models for estimating the strength of density dependence. Ecology 96:1202–1212.

Turchin, P. 2003. Complex population dynamics: a theoretical/empirical synthesis. Princeton University Press, Princeton, New Jersey, USA.

Wood, S. N. 2010. Statistical inference for noisy nonlinear ecological dynamic systems. Nature 466:1102–1104.

Zerbini, A. N., P. J. Clapham, and P. R. Wade. 2010. Assessing plausible rates of population growth in humpback whales from life-history data. Marine Biology 157:1225–1236.

Supporting Information

Additional supporting information may be found in the online version of this article at http://onlinelibrary.wiley.com/doi/10.1890/15-1406.1/suppinfo